

20. Binzel, R. P. & Xu, S. Chips off of asteroid 4 Vesta: evidence for the parent body of basaltic achondrite meteorites. *Science* **260**, 186–191 (1993).
21. Palme, H. & Rammensee, W. The significance of W in planetary differentiation processes: Evidence from new data on eucrites. *Lunar Planet. Sci.* **XXII**, 949–964 (1981).
22. Palme, H. & Beer, H. in *Landolt-Börnstein Group VI, Astronomy and Astrophysics Vol. 3a, Instruments; Methods; Solar System* (ed. Voigt, H. H.) 196–221 (Springer, Berlin, 1993).
23. Kong, P., Ebihara, M. & Palme, H. Siderophile elements in Martian meteorites and implications for core formation in Mars. *Geochim. Cosmochim. Acta* **63**, 1865–1875 (1999).
24. Newsom, H. E. *et al.* The depletion of tungsten in the bulk silicate earth: Constraints on core formation. *Geochim. Cosmochim. Acta* **60**, 1155–1169 (1996).
25. McDonough, W. F. & Sun, S.-S. The composition of the Earth. *Chem. Geol.* **120**, 223–253 (1995).
26. Wetherill, G. W. Formation of the Earth. *Annu. Rev. Earth Planet. Sci.* **18**, 205–256 (1990).
27. Canup, R. M. & Agnor, C. in *Origin of Earth and Moon* (eds Canup, R. M. & Righter, K.) 1839–1848 (Cambridge Univ. Press, Cambridge, 2001).
28. Chambers, J. E. Making more terrestrial planets. *Icarus* **152**, 205–224 (2001).
29. Münker, C., Weyer, S., Scherer, E. & Mezger, K. Separation of high field strength elements (Nb, Ta, Zr, Hf) and Lu from rock samples for MC-ICPMS measurements. *Geochem. Geophys. Geosyst.* **2**, 2001GC000183 (2001).
30. Schoenberg, R., Kamber, B. S., Collerson, K. D. & Eugster, O. New W-isotope evidence for rapid terrestrial accretion and very early core formation. *Geochim. Cosmochim. Acta* (in the press).

Acknowledgements

We thank the Muséum National d’Histoire Naturelle (Paris) for providing the meteorites Ste Marguerite and Forest Vale, the MPI Mainz for the carbonaceous chondrites, E. Scherer for discussions, and M. Drake, A. Halliday and D. Papanastassiou for comments and suggestions. This work was supported by the Deutsche Forschungsgemeinschaft as part of the research priority programme ‘Mars and the terrestrial planets’.

Competing interests statement

The authors declare that they have no competing financial interests.

Correspondence and requests for materials should be addressed to T.K. (e-mail: tkleine@nwz.uni-muenster.de).

Metal–insulator transition in chains with correlated disorder

Pedro Carpena*†, Pedro Bernal-Galván*†, Plamen Ch. Ivanov† & H. Eugene Stanley†

* *Departamento de Física Aplicada II, ETSI de Telecomunicación, Universidad de Málaga, 29071 Málaga, Spain*

† *Center for Polymer Studies and Department of Physics, Boston University, Boston, Massachusetts 02215, USA*

According to Bloch’s theorem, electronic wavefunctions in perfectly ordered crystals are extended, which implies that the probability of finding an electron is the same over the entire crystal¹. Such extended states can lead to metallic behaviour. But when disorder is introduced in the crystal, electron states can become localized, and the system can undergo a metal–insulator transition (also known as an Anderson transition)^{2–4}. Here we theoretically investigate the effect on the physical properties of the electron wavefunctions of introducing long-range correlations in the disorder in one-dimensional binary solids, and find a correlation-induced metal–insulator transition. We perform numerical simulations using a one-dimensional tight-binding model, and find a threshold value for the exponent characterizing the long-range correlations of the system. Above this threshold, and in the thermodynamic limit, the system behaves as a conductor within a broad energy band; below threshold, the system behaves as an insulator. We discuss the possible relevance of this result for electronic transport in DNA, which displays long-range correlations^{5,6} and has recently been reported to be a one-dimensional disordered conductor^{7–10}.

The tight-binding model of a solid is characterized by a hamiltonian in which one orbital (single electron) and a single energy ϵ_i

are assigned to each lattice site i

$$H = \sum_i \epsilon_i |i\rangle\langle i| + \sum_{\langle i,j \rangle} t |i\rangle\langle j| \tag{1}$$

where t is the electronic overlap (hopping term) between the wavefunctions of electrons centred at two neighbouring sites i, j . For a perfectly ordered crystal, all site energies ϵ_i have the same value or follow a periodic pattern. For disordered solids, ϵ_i can be randomly chosen from a certain probability distribution—for example, a uniform distribution or a gaussian. The probability distribution generating ϵ_i is characterized by a parameter W which quantifies the spread of the distribution, and thus the degree of disorder. In the case of a uniform distribution W is the distribution width, whereas in the case of a gaussian distribution W is the standard deviation. Models for one-dimensional (1D) disordered solids traditionally consider only two parameters of interest, namely the interaction term between nearest neighbours, t , and the disorder of the system, W . Thus the controlling parameter is the ratio W/t . Typically, t is fixed (for example, $t = 1$), thus fixing the energy scale in the system, and W is changed to study the effects produced by different levels of disorder.

In the limit $W \rightarrow 0$, where the coupling energy t between neighbours dominates, a perfect lattice is recovered, and Bloch’s theorem applies: there are extended electron states, and the system can conduct¹. This is valid for finite system size only, because localization theory asserts that in the limit of large systems all electron states are localized in the 1D case³. For sufficiently large W , where the disorder dominates, the wavefunctions are strongly localized. This localization phenomenon depends on the system dimension. For three-dimensional (3D) systems at zero temperature, $T = 0$, there is a critical value W_c for which a metal–insulator transition occurs^{11,12}. For a uniform distribution, $W_c = 16.5$. For $W < W_c$, despite some degree of disorder, the electron wavefunctions are extended, and the system behaves as a metal, whereas for $W > W_c$, the wavefunctions become localized, and the system behaves as an insulator. For two-dimensional (2D) and 1D disordered systems even infinitesimal disorder produces localized states³, so at $T = 0$ the system behaves as an insulator in the thermodynamic limit, although for some particular cases in two dimensions it is possible to find a metal–insulator transition^{13–15}.

We consider the case of a 1D system, and show that randomly chosen but long-range correlated $\{\epsilon_i\}$ can lead to extended wavefunctions and thus to conductivity, in contrast to the expectation—based on the assumption of uncorrelated disorder—that no extended states can be found in 1D disordered systems at $T = 0$ (ref. 1). Traditionally, localization of the electron wavefunction in one dimension is considered to be unaffected by the form and width of the distribution from which the $\{\epsilon_i\}$ are chosen. Although all proofs establishing localization in one dimension are model-dependent, exponential localization of all eigenstates in one dimension is believed to occur at $T = 0$ (refs 16–18). In this case, electron wavefunctions are of the form $\Psi(x) = f(x) \exp(-|x - x_0|/\lambda)$, where $f(x)$ is a random function which depends on the particular realization of the disordered chain, and λ is the localization length, which is a measure of the size of the wavefunction.

The simplest 1D model exhibiting Anderson localization is the random binary alloy¹⁹, where there are two types of atoms, A and B, and two different diagonal energies, ϵ_A and ϵ_B . To build the series of diagonal energies of the hamiltonian (equation (1)), ϵ_A and ϵ_B are assigned at random to each lattice site with probabilities p and $1 - p$, respectively. For the random binary alloy, the corresponding wavefunctions are localized and the system behaves as an insulator (Fig. 1a).

We now show that introducing correlations in the disorder can markedly change the physics. The first attempt to introduce correlations into the random binary alloy model was the random dimer model^{20,21}. In this model, short-range correlations are introduced by

assigning a dimer AA with probability p , and a monomer B with probability $1 - p$. The main property of the random dimer model is that there exists a particular energy (the resonant energy of the dimer) for which there is perfect electron transmission through the system. Wavefunctions corresponding to energies close to this resonant energy behave as extended states^{20,21}, although they do not form an energy band.

A recent attempt to introduce long-range correlations in 1D systems utilizes $\{\varepsilon_i\}$ drawn from a continuous probability distribution²². Because in this case the fluctuations in the diagonal energies (and thus the disorder in the system) increase with the system size, this work was limited to finite systems, and found

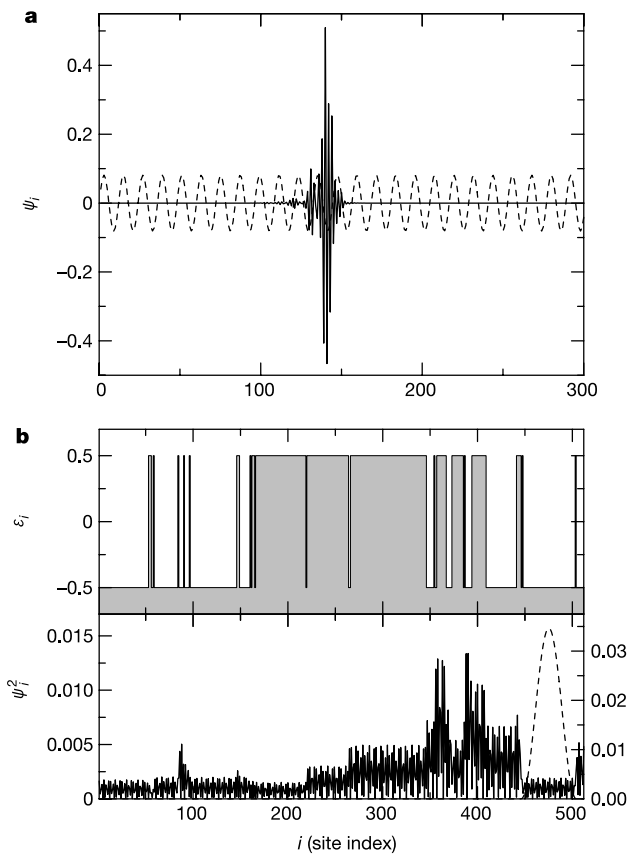


Figure 1 Wavefunctions for periodic, disordered and correlated-disordered chains. **a**, Typical wavefunctions for a periodic binary chain (dashed line) spreading over the whole system and for a random binary alloy (solid line) localized in a small region. Both are calculated for a system of size $N = 300$ atoms, and for $\varepsilon_A = 1/2$ and $\varepsilon_B = -1/2$. The wavefunctions are obtained by means of numerical diagonalization of the hamiltonian (equation (1)). **b**, Top panel: energy profile realization for a binary chain of $N = 512$ atoms with correlation exponent $\alpha = 1.2 < \alpha_c$. Bottom panel: two typical wavefunctions corresponding to a localized and a nearly extended state obtained by numerical diagonalization of the hamiltonian for the profile shown in the top panel. The localized state (dashed line) which corresponds to an energy $E = -1.5372$, randomly chosen outside the conducting band $[-1.5, 1.5]$, is different from zero only inside a cluster of identical B atoms with $\varepsilon_B = -1/2$ shown in the top panel. Out of this cluster the wavefunction becomes zero, indicating that the electron is localized and confined inside the cluster — a behaviour typical of disordered systems. However, for the nearly extended state, which correspond to an energy $E = 0.05421$ inside the central band, a very strong coupling mechanism among different correlated clusters is observed, and the wavefunction (solid line) is clearly different from zero almost everywhere, indicating delocalization of the electron even when $\alpha < \alpha_c$. This coupling mechanism is responsible for the electronic delocalization, and it only occurs in the presence of correlations and for electron states corresponding to the central energy band. The vertical scale on the left axis corresponds to the extended wavefunction, and the right axis to the localized one.

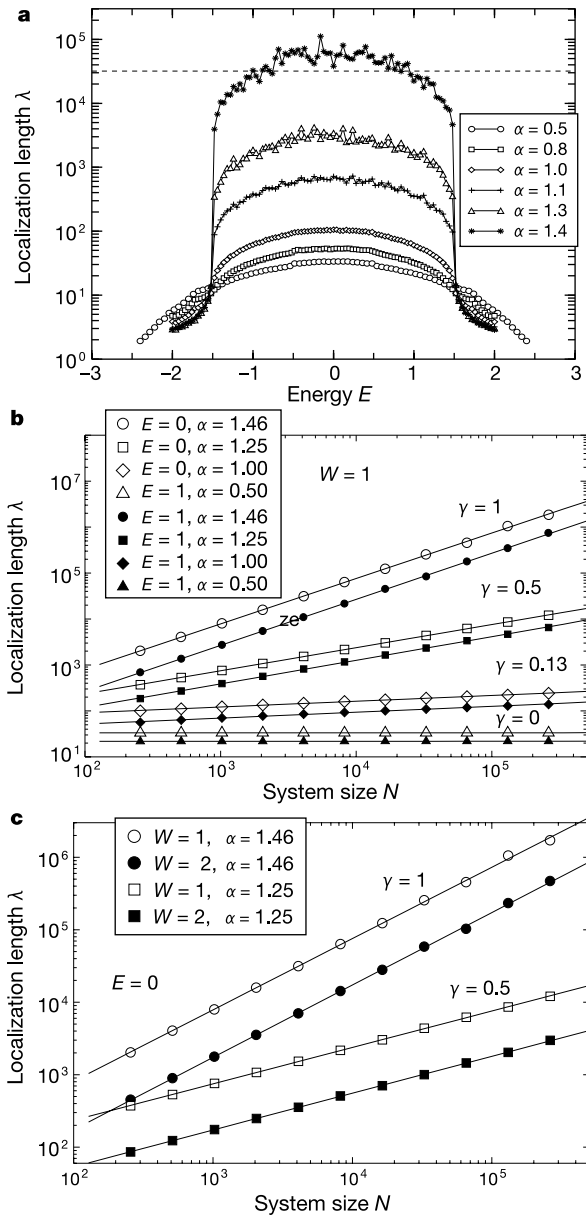


Figure 2 Localization length behaviour in correlated-disordered chains. **a**, Behaviour of the localization length λ as a function of energy E for several values of the correlations. The horizontal dashed line corresponds to the fixed system size $N = 2^{15} \approx 3 \times 10^4$. For $\alpha \approx 1.4$ we find a threshold above which extended (delocalized) states with $\lambda \approx N$ exist in the central region of the energy band $[\varepsilon_A - 2t, \varepsilon_A + 2t] \cap [\varepsilon_B - 2t, \varepsilon_B + 2t]$. As $t = 1$, $\varepsilon_A = -\varepsilon_B = 1/2$, this energy band is $[-1.5, 1.5]$. **b**, Scaling relation $\lambda \propto N^\gamma$ for different values of the correlation exponent α . This behaviour is identical for all energy values in the central band $-1.5 < E < 1.5$. We show results for $E = 0$ and $E = 1$ while keeping the disorder parameter fixed at $W = 1$. To avoid numerical fluctuations, λ is averaged in a small window of width $\Delta E = 0.1$ around each energy value. N ranges from 2^8 to 2^{18} atoms. The solid lines correspond to fits of the type $\lambda \propto N^\gamma$, from where the exponent γ is obtained. For a random binary chain with $\alpha = 0.5$, λ remains constant for all values of N and correspondingly $\gamma = 0$. For a correlated binary chain with $\alpha > \alpha_c$ we find $\gamma = 1$, indicating that above the ‘critical point’ of the metal–insulator transition the localization length is of the size of the system N . Note that, although λ is smaller for $E = 1$ compared to $E = 0$ for all α , the exponent γ remains unchanged. Thus the observed quantum insulator–metal transition is indeed valid in the thermodynamic limit and for a broad energy band. **c**, λ as a function of N for different degrees of disorder $W = |\varepsilon_A - \varepsilon_B|$ and for fixed $E = 0$. Although the system with higher disorder (filled symbols) exhibits shorter localization lengths for all system sizes, the scaling property $\lambda \propto N^\gamma$ is not altered with W , for all values of α . Thus independently of W (provided there is an intersection between the bands of A and B) the system exhibits an insulator–conductor transition for $\alpha > \alpha_c$ in the thermodynamic limit.

extended states with increasing strength of the correlations only for $E \rightarrow 0$. In order to control the disorder and to maintain the spread of the density of states, a normalization to unit standard deviation is needed, which ultimately eliminates the correlations in the ε_i and produces a series of energies that tend to be constant²³.

We propose a binary 1D model of correlated disorder, which generates a broad energy band of extended states and leads to conductivity even in the thermodynamic limit of large system size. For a perfectly ordered 1D system with atoms of only type A, the energy spectra of the solid form a single energy band $[\varepsilon_A - 2t, \varepsilon_A + 2t]$, $W/t = 0$, and we have a perfect conductor. For a random binary solid, $W \equiv |\varepsilon_A - \varepsilon_B|$. The closer the values of ε_A and ε_B are, the smaller is the ratio W/t , and the conducting properties of the disordered solid become similar to those of the perfectly ordered solid. The larger W is, the stronger is the localization. We choose $W/t = 1$, and we have strong localization in the case of pure disorder. For long-range power-law correlations in the diagonal energies ε_i , we still have $W/t = 1$. Thus, we are able to obtain extended states by keeping the level of disorder fixed, which allows conducting behaviour in the thermodynamic limit and in a broad energy band.

We generate binary sequences with long-range correlations using the modified Fourier filter method²⁴, and we use these sequences as the $\{\varepsilon_i\}$ in the binary chain. The algorithm generates random noise in the frequency domain, multiplies this noise by a power-law with the desired exponent, and then Fourier-transforms the signal back into real space. As we must generate a binary sequence, we consider a transformation which maps any positive value of the correlated series into ε_A , and any negative value into ε_B . Such a mapping can change the correlation properties of the series, and therefore the correlations are not properly quantified by the power-law exponent in the original correlated series. To quantify the correlations in the final binary sequence, we calculate the scaling exponent α using detrended fluctuation analysis^{25,26}. A value of $\alpha = 0.5$ corresponds to an uncorrelated random sequence (white noise). If $\alpha < 0.5$, the binary sequence is anticorrelated, while if $\alpha > 0.5$, there are positive long-range correlations (Supplementary Information).

Next, we study the effect of long-range power-law correlations on the localization properties of disordered binary chains. We calculate λ using the transfer matrix method¹¹. The Schrödinger equation for the hamiltonian (equation (1)) becomes

$$E\psi_n = t\psi_{n-1} + \varepsilon_n\psi_n + t\psi_{n+1} \quad (2)$$

where E is the energy corresponding to the electron wavefunction, $|\psi_n|^2$ is the probability of finding an electron at site n in the chain, and $\varepsilon_n = \varepsilon_A$ or ε_B (Fig. 1b). Using the transfer matrix method, we write equation (2) in the recursive form:

$$M_n \begin{pmatrix} \psi_n \\ \psi_{n-1} \end{pmatrix} = \begin{pmatrix} \psi_{n+1} \\ \psi_n \end{pmatrix}, \quad M_n = \begin{pmatrix} E - \varepsilon_n & -t \\ t & 0 \end{pmatrix} \quad (3)$$

The localization length $\lambda(E)$ is then defined by

$$\frac{1}{\lambda(E)} = \lim_{N \rightarrow \infty} \frac{1}{N} \ln \left| \frac{\psi_N}{\psi_0} \right| \quad (4)$$

where N is the chain length. We choose $\psi_0 = \psi_1 = 1/\sqrt{2}$. For every realization of the potential we apply equation (3) to obtain ψ_N , and we calculate $\lambda(E)$ from equation (4). We average λ over a large ensemble of realizations for a fixed system size N and fixed value of the energy E . We repeat this procedure for different values of N and E .

Our results for λ show that correlations in the sequence of $\{\varepsilon_i\}$ in the binary chain strongly modify the localization properties of the wavefunctions (Fig. 2). For $\alpha = 0.5$ and fixed N , we obtain the shortest localization length as a function of E , which corresponds to the result for a random binary alloy¹⁹. We find that long-range correlations ($\alpha' > 0.5$) change drastically the localization proper-

ties of the electronic states. When we increase the long-range correlations in the chain, λ increases in the central region of the energy band, and eventually, for a fixed N , we find a critical value α_c above which $\lambda > N$, which corresponds to extended wavefunctions (Fig. 2a). The energy region $[\varepsilon_A - 2t, \varepsilon_A + 2t] \cap [\varepsilon_B - 2t, \varepsilon_B + 2t]$ in which this increase of λ takes place is precisely the overlap of the energy bands corresponding to ordered chains formed only by A atoms and only by B atoms, so we obtain a broad band of extended states. In the random dimer model^{20,21}, there is only a single energy value that corresponds to an extended state, implying that the probability of an electron having precisely this energy is small for

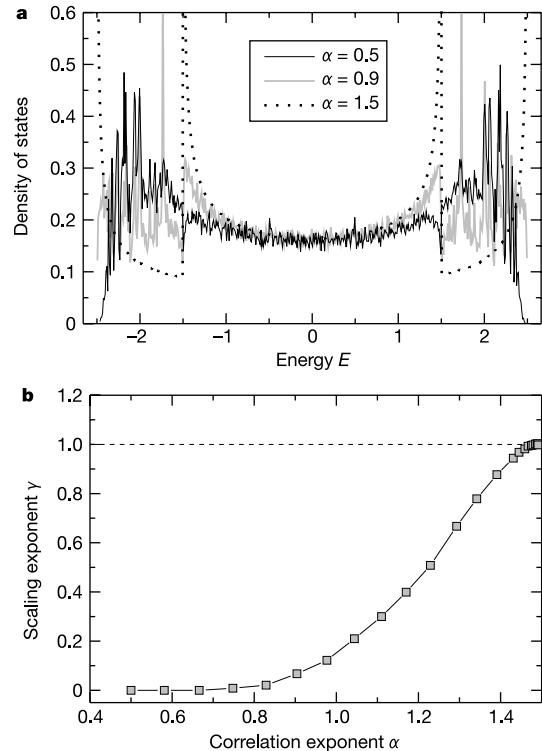


Figure 3 Density of states and scaling exponent as a function of the correlations. **a**, Density of states as a function of energy for three different values of the correlation exponent α and for $N = 2^{16}$. As the strength of the correlations increases (that is, larger values of α), there is (1) a migration of electron states to the central region $-1.5 < E < 1.5$ where the delocalization takes place, and (2) the density of states approaches the form expected for a system of two semi-infinite clusters of type A and B—four peaks with central conducting region (Fig. 2a). This reflects the fact that with increasing α the probability of finding large clusters of type A or type B in the system with correlated disorder also increases, although clusters of all sizes are present (Supplementary Information). We find that the delocalized states (conducting electrons) form a substantial fraction of the total number of electron states, and that this fraction increases with α —52.5% for $\alpha = 0.5$, 57.8% for $\alpha = 0.9$ and 66.6% for $\alpha = 1.5$. For given α the fraction of delocalized states remains the same with varying system size N . Thus for $\alpha > \alpha_c$ the majority of electron states are extended and the system exhibits metallic behaviour. **b**, The scaling exponent γ as a function of α . The value $\gamma = 1$, which corresponds to extended (delocalized) electron states in the limit $N \rightarrow \infty$, is obtained for $\alpha \approx 1.45$, suggesting a critical point at which there is transition from insulating to metallic behaviour. Note that the observed enhanced conductivity and quantum metal–insulator transition in 1D binary systems with long-range correlations is not a trivial consequence of the presence of long repetitive sequences of atoms of type A followed by long repetitive sequences of atoms B, provided the energy bands of A and B overlap. Even in the presence of very strong correlations, there is a mixture of both small and large clusters of type A and B. This is not surprising, as the correlations we introduce in the system are power-law long-range correlations, and thus the energy profile is self-similar on different size scales. Our results suggest that this self-similar organization of clusters of different size can lead to extended states and metal–insulator transition.

finite systems, and becomes zero in the thermodynamic limit of large system size. In contrast, long-range power-law correlations produce a broad conducting energy band. Moreover, the population of this central band increases with the correlations, ranging from

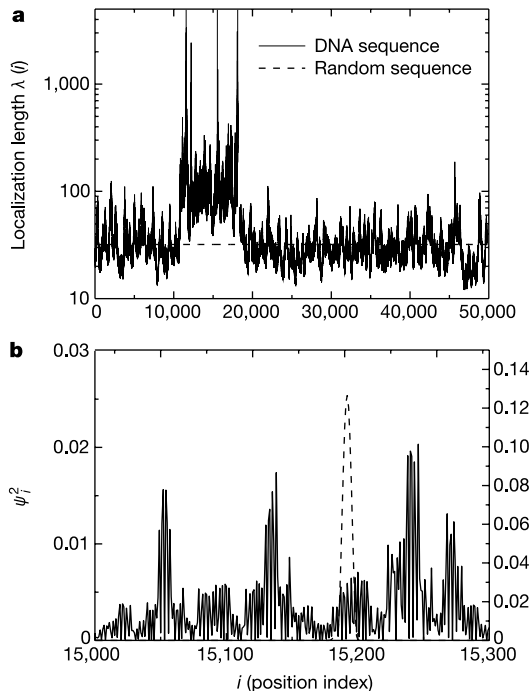


Figure 4 Results in DNA. **a**, λ as a function of the position in a DNA sequence. We present the following experiment: (1) We select a DNA sequence corresponding to the first 50,000 nucleotides of the largest contig (a perfectly sequenced region without gaps) of human chromosome 22 (NT_011520) retrieved from the National Center for Biotechnology Information (NCBI). (2) We map this sequence onto a binary alphabet so that nucleotides A and T gives $\epsilon_A = 1/2$ and nucleotides C and G give $\epsilon_B = -1/2$ to construct the diagonal energies in the hamiltonian (equation (1)). (3) We divide the sequence into overlapping subsequences of size $N = 300$, one for each nucleotide in the original DNA sequence (that is, for nucleotide i we consider the subsequence between $[i, i + 299]$), and we calculate λ for $E = 0$ and for each i . (4) We plot λ as a function of the sequence position i . Note that there is a certain region of non-repetitive DNA comprising $N \approx 8,000$ nucleotides and characterized by strong long-range correlations with $\alpha \approx 0.9$. For this region, we find that λ is on average ten times greater compared to the neighbouring segments of DNA where there are no strong correlations, and compared to a surrogate random sequence (horizontal dashed line). Thus electron transport in DNA can be clearly enhanced owing to long-range correlations, leading to conductivity over DNA segments comprising hundreds or even thousands of nucleotides. Looking for segments of DNA from the human chromosome 22 which have similar correlation properties and enhanced electron transport, we found that the biological function of these segments is not provided and is not known. Perhaps the patterns formed by segments with particular conduction (correlation) properties can provide a clue to understanding their biological function. **b**, Two wavefunctions corresponding to a subsequence of length $N = 300$ located at $i = 15,000$, as described in **a**. The wavefunctions are obtained by numerical diagonalization of the hamiltonian in equation (1) with diagonal energies corresponding precisely to these 300 nucleotides. The solid line (left vertical axis) represents a nearly extended state corresponding to an energy value $E = -0.17753$ from the central band $[-1.5, 1.5]$, and the dotted line (right vertical axis) shows a strongly localized state corresponding to $E = 1.55761$ outside the central band. Whereas the localized state is confined within ~ 30 base pairs, the extended state allows for an electron transport throughout the sequence. Moreover, because λ exceeds the size of the segments with correlated disorder, the electron wavefunction overlaps with parts of the neighbouring uncorrelated disordered segments and can affect their conducting properties, thus facilitating important genomic functions²⁷. Note the similarity between this plot obtained for DNA and the wavefunction in Fig. 1b obtained for a computer-generated correlated binary sequence.

52% for $\alpha = 0.5$ to 67% for $\alpha = 1.5$ (Fig. 3a). Thus, the probability of an electron propagating throughout the system, which is proportional to the width of the conducting energy band, is not small, and the conducting behaviour resembles a metal.

To speak properly of extended states, we need the condition $\lim_{N \rightarrow \infty} (\lambda/N) = \text{constant} \neq 0$. If this condition is not fulfilled, λ becomes negligible in comparison to N in the thermodynamic limit $N \rightarrow \infty$, and the wavefunction is therefore localized. Hence, we next study the behaviour of λ as a function of N for different values of the correlations. As λ is also a function of the electron energy E , we choose $E = 0$ —that is, the central energy of the band. To avoid excessive numerical fluctuations, we average λ in a small energy window around $E = 0$, specifically the interval $[-0.05, 0.05]$. We find a power-law relation between λ and N , $\lambda \propto N^\gamma$ (Fig. 2b, c), where the exponent γ depends on the correlation exponent α (Fig. 3b). Our results for the values of $\lambda(E)$ (Fig. 2a) indicate a nearly flat plateau covering the central energy band, suggesting that a similar relation between λ and N can be expected for every other value of E in this energy interval. Indeed, for all $E \in [-1.5, 1.5]$ we find the same values of γ (Fig. 2b).

Further, we find that γ is also independent of W (Fig. 2c). As W is fixed, introducing power-law correlations in the chain leads to re-ordering of the diagonal energy values ϵ_i to produce clusters the sizes of which are power-law distributed (Supplementary Information), and at the same time not changing the level of disorder when N varies. We find that a change in W modifies the values of λ : λ decreases with increasing W . But owing to the power-law correlations, the fraction λ/N remains constant when $N \rightarrow \infty$ (note the constant vertical shift in Fig. 2c), while the scaling relation, $\lambda \propto N^\gamma$, does not change with W . Thus, in the thermodynamic limit, this scaling behaviour is independent of the level of disorder.

For values of $\alpha \approx 0.5$ we find that $\gamma \approx 0$, so we have localized states. As α increases, γ also increases; for $\alpha \geq 1.45$ we obtain $\gamma = 1$ within our error bars (Fig. 3b). Therefore, at $T = 0$ and in the limit $N \rightarrow \infty$, for $\alpha < 1.45$, the system behaves as an insulator, while for $\alpha > 1.45$ the system behaves as a conductor within a broad energy band. For $\alpha = \alpha_c = 1.45$, we find a new ‘critical point’ at which a quantum metal–insulator transition occurs.

These findings can be used to better understand the conduction properties in 1D disordered binary solids, which are important for practical applications such as the construction of nanoscopic electronic devices⁹. Electrical conduction in biological macromolecules, in particular DNA, has also attracted much attention. Recent work has shown that electrons or holes are responsible for the electrical current in DNA^{7–10}. Moreover, it has been observed that certain mutation repairs occur in natural DNA by means of electrical current transport along the molecule²⁷. Experiments of DNA conductivity find conducting^{7,28}, semiconducting⁹ and insulating²⁹ behaviour, due perhaps to the different type of DNA sequences considered—random, repetitive or correlated. An open question is the influence of the ‘ordering’ (that is, correlations) of the DNA nucleotides on the conduction properties of the sequence.

In DNA, correlations with exponent $\alpha \approx \alpha_c$ do not exist. Typical values of α in DNA range between 0.6 and 0.9 (refs 5, 6), which are below α_c but are significantly greater than the value of 0.5 for purely random sequences. Our results show that such long-range correlations can strongly affect the electronic transport over relatively large distances. In particular, we consider a sequence of 50,000 nucleotides of the largest contig of human chromosome 22 (Fig. 4). We find that for non-repetitive regions with long-range correlations, the localization length obtained with our model when the DNA is mapped onto a binary chain is between one and two orders of magnitude greater (Fig. 4a) than that expected for a random sequence (Fig. 2a, b). This behaviour is also reflected in the fact that we obtain nearly extended wavefunctions for all energy values from the central band of the DNA sequence (Fig. 4b). Recent experiments show that random DNA is not a good conductor²⁹, whereas

repetitive DNA conducts quite well³⁰—both cases are in agreement with our model (Figs 2 and 3). Further, our results suggest that in non-repetitive long-range correlated regions of DNA, electrons can propagate over average distances of ~300 nucleotides, and that a fraction can propagate over distances of more than 1,000 nucleotides. In fact, the DNA segment in Fig. 4a, where our model predicts very good conducting behaviour, is even longer—extending to ~8,000 nucleotides. This conducting behaviour does not imply that correlated DNA is a macroscopic conductor, but rather that electronic transport at moderate distances can be found at $T = 0$. This distance range (~1 μm) is the focus of the above-mentioned experiments.

In summary, we find that long-range correlations change the localization properties of 1D disordered binary solids. We show that the localization length of the electron wavefunction is greatly increased by long-range correlations. In addition, for correlations stronger than a certain threshold, we find in the thermodynamic limit a broad energy band of extended states, and therefore a conducting phase. Thus, although still disordered, the 1D system can behave as a conductor; in contrast to the traditional theory which is applicable only for uncorrelated disorder. The threshold in the control parameter (the value of the correlation exponent) corresponds to a ‘critical point’ at which a metal–insulator transition takes place. These findings may be of importance for elucidating the electronic transport and the biological function of DNA segments with different types of correlations, as well as for the design of nanoscopic devices. □

Received 1 May; accepted 28 June 2002; doi:10.1038/nature00948.

1. Ashcroft, N. W. & Mermin, N. D. *Solid State Physics* (Holt-Saunders, London, 1976).
2. Anderson, P. W. Absence of diffusion in certain random lattices. *Phys. Rev.* **109**, 1492–1505 (1958).
3. Kramer, B. & MacKinnon, A. Localization: theory and experiment. *Rep. Prog. Phys.* **56**, 1469–1564 (1993).
4. Janssen, M. Statistics and scaling in disordered mesoscopic electron-systems. *Phys. Rep.* **295**, 1–91 (1998).
5. Peng, C.-K. *et al.* Long-range correlations in nucleotide sequences. *Nature* **356**, 168–170 (1992).
6. Holste, D., Grosse, I. & Herzel, H. Statistical analysis of the DNA sequence of human chromosome 22. *Phys. Rev. E* **64**, 041917 (2001).
7. Fink, H. V. & Schönenberger, C. Electrical conduction through DNA molecules. *Nature* **398**, 407–410 (1999).
8. Henderson, P. T., Jones, D., Hampikian, G., Kan, Y. & Schuster, G. B. Long distance charge transport in duplex DNA: The phonon-assisted polaron-like hopping mechanism. *Proc. Natl Acad. Sci. USA* **96**, 8353–8358 (1999).
9. Porath, D., Bezryadin, A., de Vries, S. & Dekker, C. Direct measurement of electrical transport through DNA molecules. *Nature* **403**, 635–638 (2000).
10. Hjort, M. & Stafstrom, S. Band resonant tunnelling in DNA molecules. *Phys. Rev. Lett.* **87**, 228101 (2001).
11. Mackinnon, A. & Kramer, B. One-parameter scaling of localization length and conductance in disordered systems. *Phys. Rev. Lett.* **47**, 1546–1549 (1981).
12. Hofstadter, E. & Schreiber, M. Statistical properties of the eigenvalue spectrum of the three-dimensional Anderson hamiltonian. *Phys. Rev. B* **48**, 16979–16985 (1993).
13. Kravchenko, S. V., Simonian, D., Sarachik, M. P., Mason, W. & Furneaux, J. E. Electric-field scaling at $B = 0$ metal-insulator transition in 2 dimensions. *Phys. Rev. Lett.* **77**, 4398–4941 (1996).
14. Weymer, A. & Janssen, M. Localization length exponent, critical conductance distribution and multifractality in hierarchical networks models for the quantum Hall-effect. *Ann. Phys. (Leipzig)* **7**, 159–173 (1998).
15. Schweitzer, L. & Zharekeshev, I. Kh. Scaling of level statistics and critical exponent of disordered 2-dimensional symplectic systems. *J. Phys. Condens. Matter* **9**, L441–L445 (1997).
16. Mott, N. F. & Twose, W. The theory of impurity conduction. *Adv. Phys.* **10**, 107–163 (1961).
17. Abou-Chacra, R., Anderson, P. W. & Thouless, D. J. A selfconsistent theory of localization. *J. Phys. C*, **6**, 1734–1752 (1973).
18. Ishii, K. & Matsuda, H. Localization of normal modes and energy transport in the disordered harmonic chain. *Prog. Theor. Phys. Suppl.* **45**, 56–86 (1970).
19. Davids, P. S. Lyapunov exponents and transfer-matrix spectrum of the random binary alloy. *Phys. Rev. B* **52**, 4146–4155 (1995).
20. Dunlap, D. H., Wu, H.-L. & Phillips, P. Absence of localization in a random-dimer model. *Phys. Rev. Lett.* **65**, 88–91 (1990).
21. Phillips, P. & Wu, H.-L. Localization and its absence: a new metallic state for conducting polymers. *Science* **252**, 1805–1812 (1991).
22. de Moura, F. A. B. F. & Lyra, M. L. Delocalization in the 1D Anderson model with long-range correlated disorder. *Phys. Rev. Lett.* **81**, 3735–3738 (1998).
23. Kantelhardt, J. W., Russ, S., Bunde, A., Havlin, S. & Webman, I. Comment on delocalization in the 1D Anderson model with long-range correlated disorder. *Phys. Rev. Lett.* **84**, 198–201 (2000).
24. Makse, H. A., Havlin, S., Schwartz, M. & Stanley, H. E. Method for generating long-range correlations for large systems. *Phys. Rev. E* **53**, 5445–5449 (1996).
25. Hu, K., Ivanov, P. Ch., Chen, Z., Carpena, P. & Stanley, H. E. Effect of trends on detrended fluctuation analysis. *Phys. Rev. E* **64**, 011114 (2001).

26. Chen, Z., Ivanov, P. Ch., Hu, K. & Stanley, H. E. Effect of nonstationarities on detrended fluctuation analysis. *Phys. Rev. E* **65**, 041107 (2002).
27. Dandliker, P. J., Holmlin, R. E. & Barton, J. K. Oxidative thymine dimer repair in the DNA helix. *Science* **275**, 1465–1468 (1997).
28. Kasumov, A. I. *et al.* Proximity-induced superconductivity in DNA. *Science* **291**, 280–282 (2001).
29. de Pablo, P. J. *et al.* Absence of dc-conductivity in λ -DNA. *Phys. Rev. Lett.* **85**, 4992–4995 (2000).
30. Yoo, K.-H. *et al.* Electrical conduction through poly(dA)-poly(dT) and poly(dG)-poly(dC) DNA molecules. *Phys. Rev. Lett.* **87**, 198102 (2001).

Supplementary information accompanies the paper on Nature’s website (<http://www.nature.com/nature>).

Acknowledgements

We thank L. Cruz for discussions, and the Spanish Ministerio de Educación y Cultura and NIH/National Center for Research Resources for support.

Competing interests statement

The authors declare that they have no competing financial interests.

Correspondence and requests for materials should be addressed to P.C. (e-mail: pcarpena@ctima.uma.es or pjcarpena@uma.es).

.....
Near-infrared sensitivity enhancement of photorefractive polymer composites by pre-illumination

Erwin Mecher*, **Francisco Gallego-Gómez*†**, **Hartwig Tillmann‡**, **Hans-Heinrich Hörhold‡**, **Jan C. Hummelen§** & **Klaus Meerholz*†**

* *Chemistry Department and Center for Nanoscience (CeNS), University of Munich, Butenandtstrasse 11, 81377 Munich, Germany*
 ‡ *Organic and Macromolecular Chemistry, University of Jena, Humboldtstrasse 10, 07743 Jena, Germany*
 § *Stratingh Institute and Materials Science Center, University of Groningen, Nijenborgh 4, 9747 AG Groningen, The Netherlands*

.....
 Among the various applications for reversible holographic storage media^{1,2}, a particularly interesting one is time-gated holographic imaging (TGHI)^{3–5}. This technique could provide a noninvasive medical diagnosis tool, related to optical coherence tomography^{6,7}. In this technique, biological samples are illuminated within their transparency window with near-infrared light, and information about subsurface features is obtained by a detection method that distinguishes between reflected photons originating from a certain depth and those scattered from various depths. Such an application requires reversible holographic storage media with very high sensitivity in the near-infrared. Photorefractive materials, in particular certain amorphous organic systems, are in principle promising candidate media, but their sensitivity has so far been too low, mainly owing to their long response times in the near-infrared. Here we introduce an organic photorefractive material—a composite based on the poly(arylene vinylene) copolymer TPD-PPV⁸—that exhibits favourable near-infrared characteristics. We show that pre-illumination of this material at a shorter wavelength before holographic recording improves the response time by a factor of 40. This process was found to be reversible. We demonstrate multiple holographic recording with this technique at video rate under practical conditions.

† Present address: Physical Chemistry Department, University of Cologne, Luxemburgerstrasse 116, 50939 Cologne, Germany.

24. Pan, T., Loria, A. & Zhong, K. Probing of tertiary interactions in RNA: 2'-hydroxyl-base contacts between the RNase P RNA and pre-tRNA. *Proc. Natl Acad. Sci. USA* **92**, 12510–12514 (1995).
25. Loria, A. & Pan, T. Recognition of the T stem-loop of a pre-tRNA substrate by the ribozyme from *Bacillus subtilis* ribonuclease P. *Biochemistry* **36**, 6317–6325 (1997).
26. Nolan, J. M., Burke, D. H. & Pace, N. R. Circularly permuted tRNAs as specific photoaffinity probes of ribonuclease P RNA structure. *Science* **261**, 762–765 (1993).
27. Hendrickson, W. A. Determination of macromolecular structures from anomalous diffraction of synchrotron radiation. *Science* **254**, 51–58 (1991).
28. Murshudov, G. N., Vagin, A. A. & Dodson, E. J. Refinement of macromolecular structures by the maximum-likelihood method. *Acta Crystallogr. D* **53**, 240–255 (1997).
29. Brunger, A. T. *et al.* Crystallography & NMR system: a new software suite for macromolecular structure determination. *Acta Crystallogr. D* **54**, 905–921 (1998).
30. Haas, E. S., Banta, A. B., Harris, J. K., Pace, N. R. & Brown, J. W. Structure and evolution of ribonuclease P RNA in Gram-positive bacteria. *Nucleic Acids Res.* **24**, 4775–4782 (1996).

Supplementary Information accompanies the paper on *Nature's* website (<http://www.nature.com/nature>).

Acknowledgements We thank X. Liu and Y. Xiao for technical assistance, A. Changela, H. Feinberg, V. Grum and members of DND–CAT for help with data collection, and A. Changela, C. Correll, V. Grum, E. Sontheimer, B. Taneja and J. Wedekind for comments and suggestions. Research was supported by the NIH (to A.M.) and an NIH NRSA Fellowship to A.K. Support from the R.H. Lurie Cancer Center of Northwestern University to the Structural Biology Center is acknowledged. Portions of this work were performed at the DuPont–Northwestern–Dow Collaborative Access Team (DND–CAT) Synchrotron Research Center at the Advanced Photon Source (APS) and at the Stanford Synchrotron Radiation Laboratory (SSRL). DND–CAT is supported by DuPont, Dow and the NSF, and use of the APS is supported by the DOE. SSRL is operated by the DOE, Office of Basic Energy Sciences. The SSRL Biotechnology Program is supported by the NIH and the DOE.

Competing interests statement The authors declare that they have no competing financial interests.

Correspondence and requests for materials should be addressed to A.M. (e-mail: a-mondragon@northwestern.edu). Coordinates have been deposited in the Protein Data Bank under the accession code 1NBS.

retractions

A cytosolic catalase is needed to extend adult lifespan in *C. elegans* *daf-1* and *clk-1* mutants

J. Taub, J. F. Lau, C. Ma, J. H. Hahn, R. Hoque, J. Rothblatt & M. Chalfie

Nature **399**, 162–166 (1999).

We no longer have confidence in our observations associating a reduction in adult lifespan with a putative mutation in the *Caenorhabditis elegans* catalase gene *ctl-1* and therefore retract this paper. With the assistance of J. Liang and C. Keller, we have confirmed that *C. elegans* has multiple catalase genes (actually three in tandem) and that the original strain, TU1061, has decreased transcription of *ctl-1* messenger RNA. However, we have also found several errors, one identifying a single nucleotide deletion as the defect in the putative *ctl-1* mutation and others in the identification of strains carrying mutations in multiple genes. In particular, we have not seen the expected reduction in *ctl-1* mRNA in other

strains tested. The longevity results obtained with these strains are therefore meaningless. We are grateful to our colleagues, particularly C. Kenyon and M. Crowder, for conveying to us their concerns about our results. □

Metal–insulator transition in chains with correlated disorder

Pedro Carpena, Pedro Bernaola-Galván, Plamen Ch. Ivanov & H. Eugene Stanley

Nature **418**, 955–959 (2002).

This Letter reported numerical simulations of one-dimensional disordered binary systems, and found a threshold value for the exponent characterizing the long-range power-law correlations of the system. Below this threshold, the system behaves as an insulator and above it, in the thermodynamic limit, the system behaves as a conductor. Unfortunately, we have now found that this observation was a consequence of the algorithm used to generate long-range correlations in binary chains, because above the threshold value of the exponent only a finite number of segments of atoms of the same type (A or B) exists, even in the thermodynamic limit of an infinitely large system. Thus, the system studied was not truly disordered. As a result, what we observed at the critical threshold value for the correlation exponent was not a transition from insulator to metal behaviour in a disordered system (as reported), but a transition from a disordered to an ordered system. For this reason, the authors retract the claim of a metal–insulator transition in the infinite binary chain with correlated disorder. The results are still valid that relate to the behaviour of a binary chain below the critical threshold value of the correlation exponent, and to large but finite system sizes (as found in the DNA example discussed in the Letter).

We thank L. Hufnagel and T. Geisel for drawing this to our attention. □

erratum

Wave-like properties of solar supergranulation

L. Gizon, T. L. Duvall Jr & J. Schou

Nature **421**, 43–44 (2003).

In Fig. 1, the units of frequency should be microhertz (μHz), not millihertz (mHz). In the US-printed issues, Fig. 3b appeared blurred. □